Electronic Supplementary Material (ESI) for Journal of Materials Chemistry C.

Supp. Inf.

1. **Calculation of the light intensity distribution inside of the perovskite crystals**:
   Absorption law:

$$I_{z,tot} = I_0 e^{-\alpha(z-z_{surface})}$$

   Dependence on the spot area:

$$\frac{\partial I(z,x)}{\partial x} = \frac{I_{z,tot}}{\pi r^2}$$

$$r = \left(z - z_{focus}\right) * \tan(\beta)$$

   Snell's law:

$$\frac{\sin(\beta)}{\sin(\gamma)} = \frac{n_{air}}{n_{per}}$$

   End equation:

$$\frac{\partial I(z,x)}{\partial x} = \frac{I_0 e^{-\alpha(z-z_{surface})}}{\pi\left(z - z_{focus}\right)^2 * \tan\left(\frac{n_{air}}{n_{per}} * \sin(\gamma)\right)^2}$$

   With $\gamma = 53.8°$, $n_{per} = 2.4115$ *and* $\alpha =$ 1.2473 × 10^5 cm^{-1}

2. **Simulated light distribution in perovskite crystals**
   Using the relation from the previous part, we have simulated the light distribution in the perovskite crystals during PL measurements at z values of 0 µm, 30 µm and 60 µm using MATLAB software.

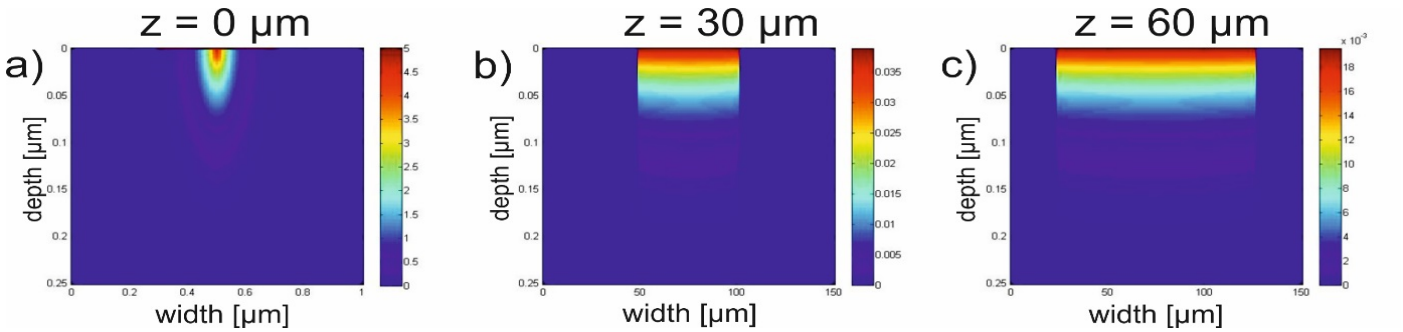

Figure 1. Simulated light distribution in perovskite crystals at a) z = 0 µm, b) z = 30 µm and c) z = 60 µm

3. **Pl signal at the GB can be fitted with 2 Gauss functions related to the band-to-band transition ad to the defect states.**

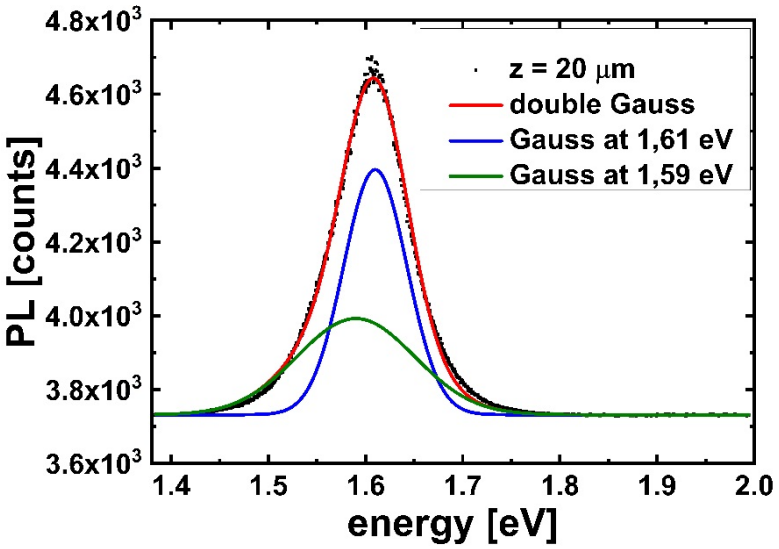

Figure 2. Double Gauss fit of the PL signal at GB

4. **PL intensity change due to the z-value change at the GB and in the bulk**.

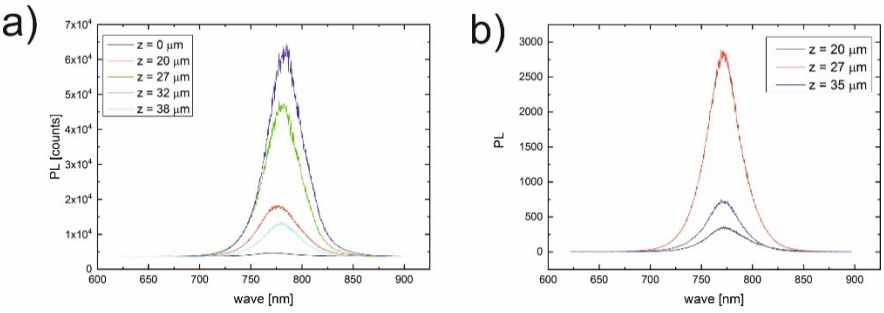

Figure 3. PL signal change at a) GB and b) bulk

We note that the enhance of the PL intensity at small z values could be explained by the decomposition of surface of perovskite at focus position due to the high energy density If z value increases, the exposed area becomes bigger and the energy density decreases. This leads to the damage-free situation.

5. **An angle dependency calibration for XPS measurements at bicrystals**

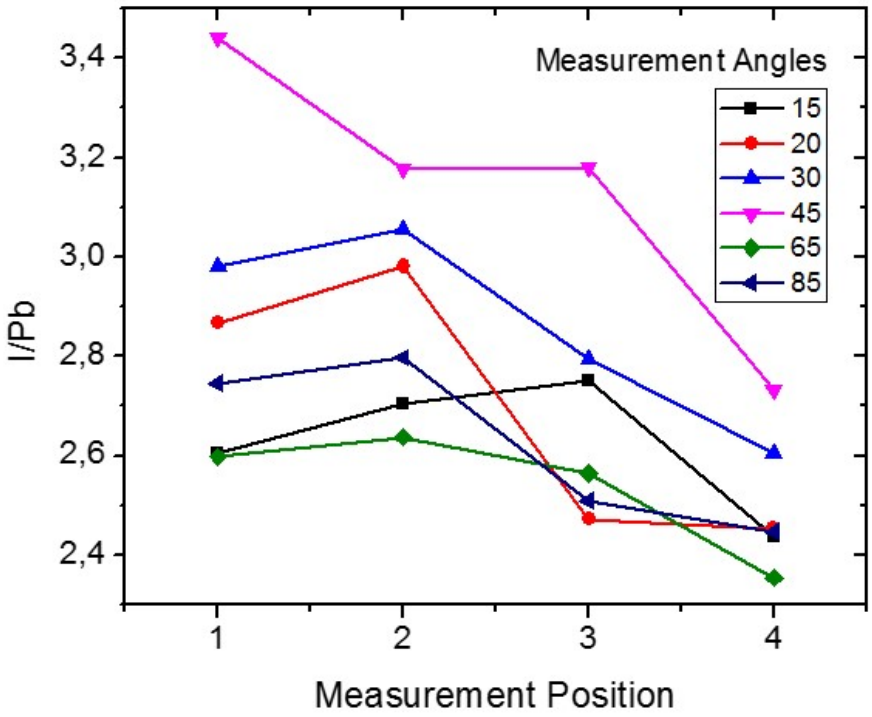

Figure 4. Iodide-lead relation at GB at different measurement angles

The absolute angle of 45° was used for the further measurements, because of the calibration described in text.

6. **Iodide spectra in µ-XPS measurements** at position 1, 2, 3, 4 respectively:

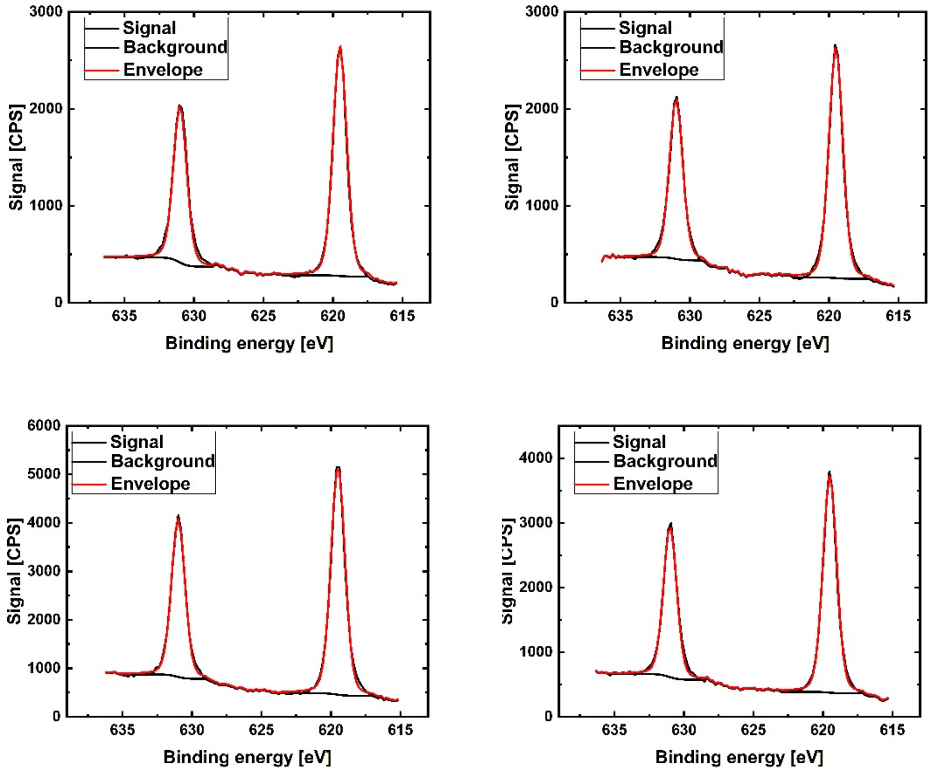

Figure 5. Iodide spectra in u-XPS measurements at positions 1, 2, 3 and 4 respectively. No iodide-iodide component is observed.

7. PL signal at the GB during defocusing/focusing:

To verify, if there is the influence of the laser exposure on the PL signal, we carried out following experiment: we have cycled the laser focus conditions on the grain boundary as shown in figure 6. Here the focus was changed from z=23µm (no red shift) to z = 44µm (PL signal red shifted) and back again to z = 24µm (no red shift). The PL signal red shift observed in the grain boundary region, is completely reversible. Because of this observation, we suppose, that no laser stimulated degradation influence the results of PL measurements.

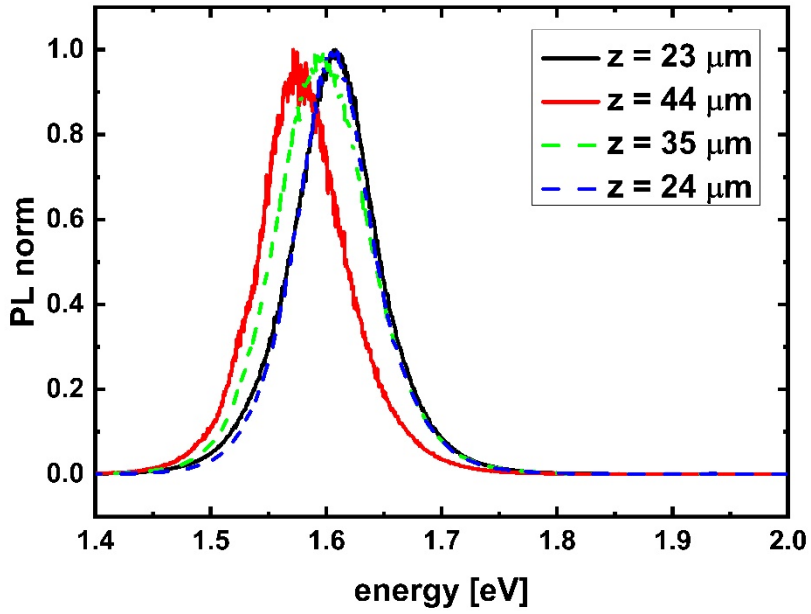

Figure 6. Focus change in both directions. At first, the z-value was changed from 23 µm to 44 µm (defocusing). Subsequently, the z value was changed back over 35 µm to 24µm. No signal change was observed between PL signals at z = 23 µm and z = 24 µm.

8. PL signal change at the GB during laser power change

To get another evidence, if the light exposure influences our results, we have evaluated the grain boundary signal for laser power values ranging from 80-106% of the initial value (it corresponds to 1.2 µW, 1.3 µW, 1.5 µW and 1.6 µW respectively), using the focus of the red shifted PL signal. This is demonstrated in the following using figure 7. While an increase in laser power leads to an enhanced PL signal, no power dependent shift in emission wavelength could be detected.

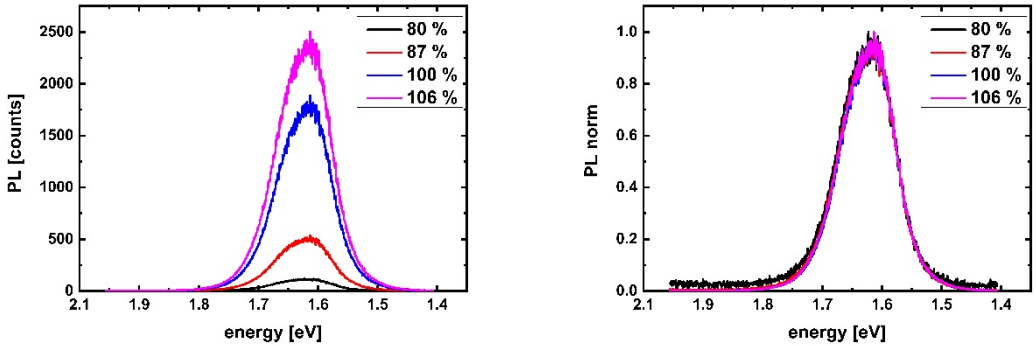

Figure 7. No change in PL signal form was observed during the laser power change

9. Repeated PL measurements at another MAPI sample

The µ-PL measurements at GB were repeated at an another bicrystal to verify the results. Here the same photoluminescence signal shift of about 30 meV was observed.

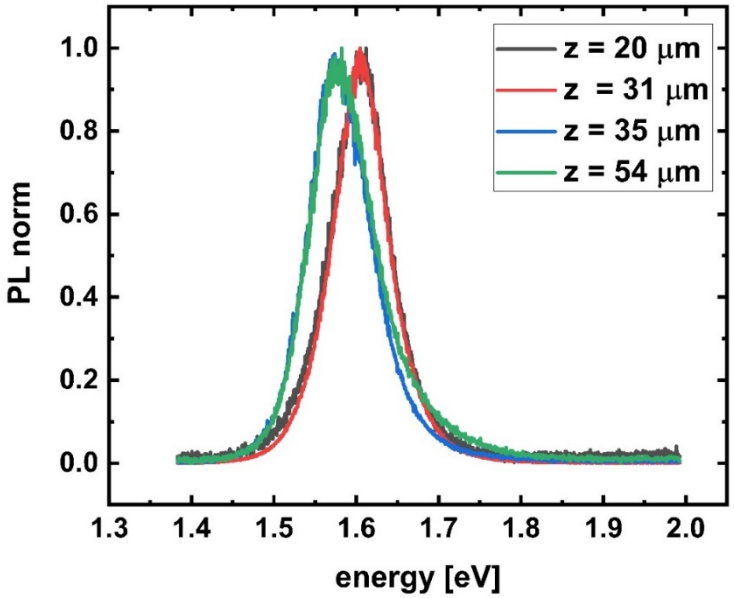

Figure 8. Figure 6 Photoluminescence shift at another bicrystal

10. Repeated XPS measurements at another MAPI sample

We repeated the XPS (without angle dependence) using other samples, to verify our method. As expected, we have observed a similar dependence of the I/Pb, Pb/N and I/N concertation on the distance from the GB using 3 different grain boundaries, which confirms the correctness of our findings. This is illustrated in figure 10. The observed fluctuations in the constituent ratios are the consequence of the angle dependence, which is already discussed in the manuscript. The only deviation with respect to our original experiments, is the presence of a small amount of CH_3I impurities (~5% of the iodide signal), as depicted in the I3d spectrum of figure 9, which is ascribed to solvent residue on the crystal surface. This impurity does not influence the interpretation of our experiment, as the influence on the I/Pb ratio is low. This is illustrated in figure 10d).

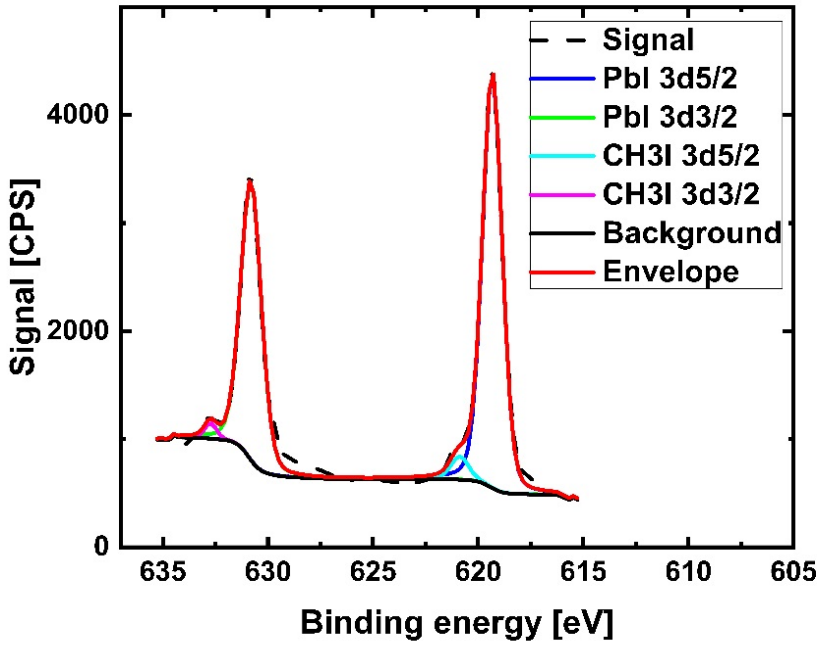

Figure 9. Two peaks are detected in the iodide signal. The peaks with maxima at 619.4 eV and 630.9 eV are ascribed to the PbI compound. The peaks at 620.8 eV and 632.5eV are ascribed to CH3I compound

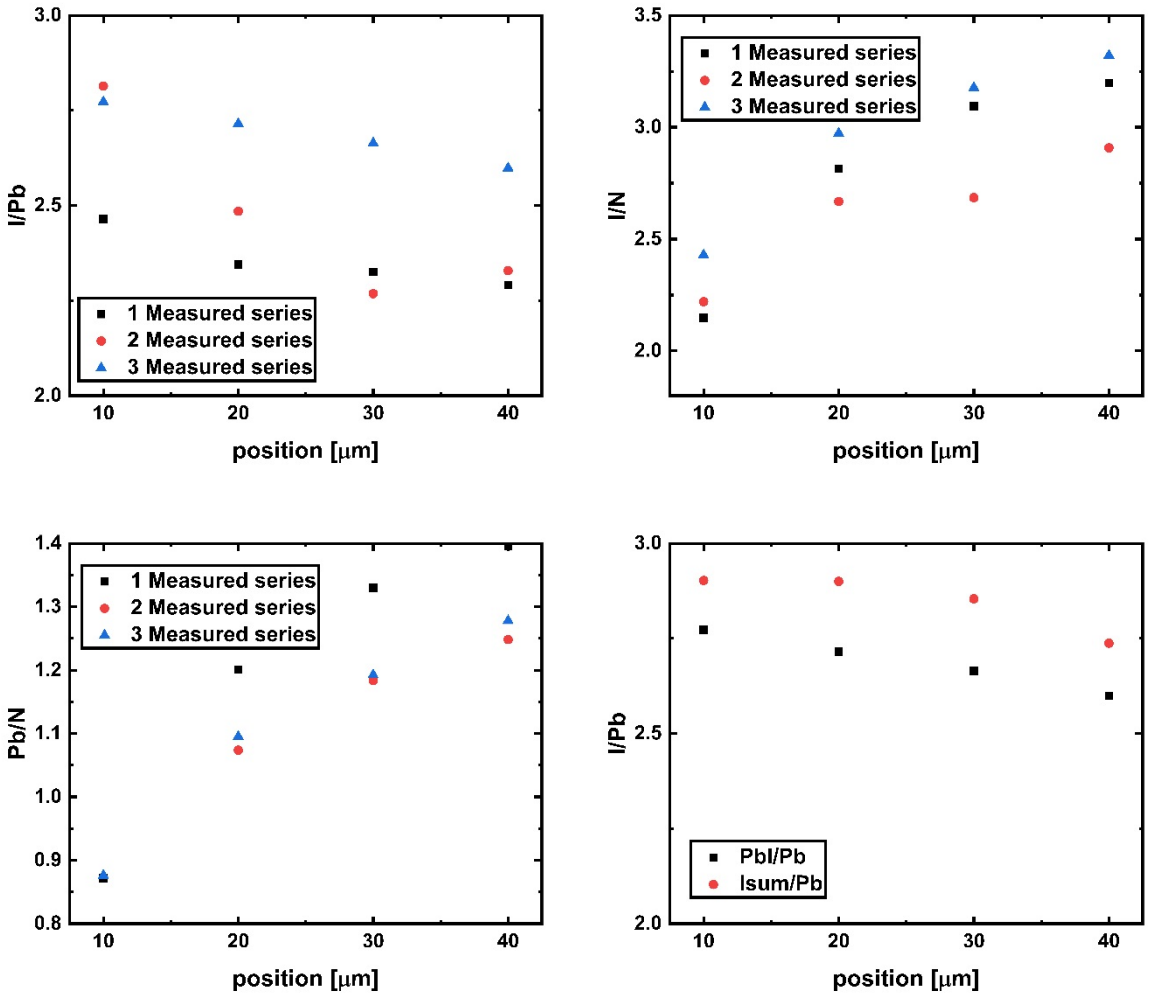

Figure 10. (a)Iodide-lead, (b) iodide-nitrogen and (c) lead-nitrogen relations at different distances at 3 different grain boundaries at an absolute angle of 45°. (d) The change of the iodide-lead relation if the total iodide signal is considered.

11. SEM micrographs of investigated crystals

For our investigation, we have grown the crystallites according to the process / recipe outlined in the "Nature Communications" publication by Saidaminov et al.[1] As this publication substantiates the single crystalline nature of the grown solids, it is a good assumption that our own crystals would have a similar quality. We have used the same experiment as described by Saidaminov et al.[1] to support this assumption. To get a strong indication, that our crystallites are indeed single crystals fused together, a SEM analysis of the crystal top view, as well as of the cleaved cross section was conducted. The result of the top view analysis is illustrated in figure 11 a) and b). Neither in the low-resolution (a) nor in the high-resolution (b) micrographs are grain boundaries visible, which would indicate a polycrystalline solid structure. An amorphous structure can be excluded by considering the well-defined form of the individual crystals grown together (Fig. 11 a). This result is supported by considering the side view of the cleaved crystallite illustrated in figure 12 a) and b). The structural irregularities shown in a) are the result of knife damage, which was

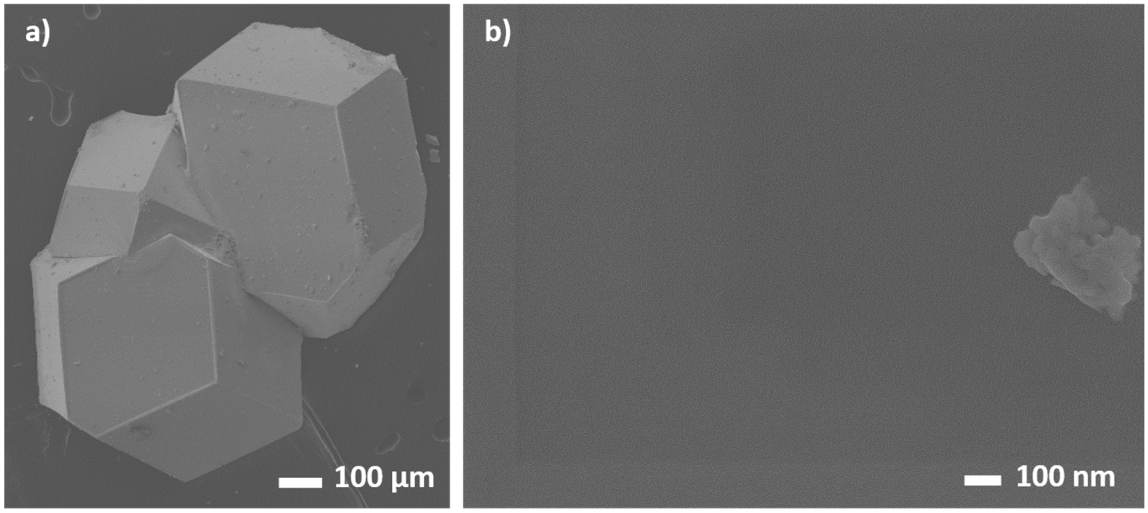

Figure 11. (a) Low-resolution and (b) high-resolution SEM micrographs of MAPI crystal surface fabricated using recipe of Saidaminov et. al. No grain boundaries were observed at the surface of crystals.

used in the cleaving process. The high-resolution micrograph of a clean area shown in b), shows no indication for grain boundaries, resulting a case for the suggested single crystalline nature of the solid.

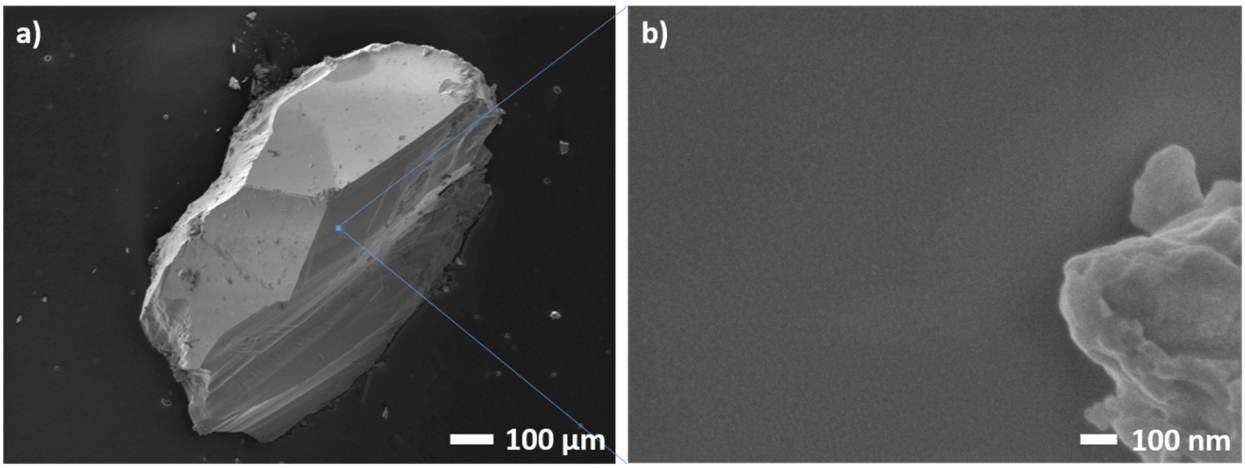

Figure 12. (a) Low-resolution and (b) high-resolution SEM micrographs of cleaved MAPI crystals fabricated using recipe of Saidaminov et. al. No grain boundaries were observed in crystals.

12. XRD pattern of investigated MAPI samples

To demonstrate the crystallinity of our samples XRD measurements were conducted. For these measurements, the crystals were milled to powder and subsequently filled into a glass capillary (diameter 0.3 mm). The X-ray powder pattern for qualitative phase analysis was collected on a Stoe STADI P transmission diffractometer using Mo radiation (0.7093 Å). The instrument is equipped with a primary Ge (111) monochromator (MoKα1) and a position sensitive Mythen1K detector. Data was collected in the range between 2 and 30° 2θ with a step width of 0.015° 2θ. Measuring time per step was 20 s, 6 scans were collected and summed after data collection. The measured pattern (Black Line) was evaluated qualitatively

by comparison with entries for the MAPI constituents from the ICCD PDF-2 powder pattern database (Red Line). We find a good agreement for the data, allowing us to conclude that we have indeed an ideal MAPI Phase in the individual crystallites.

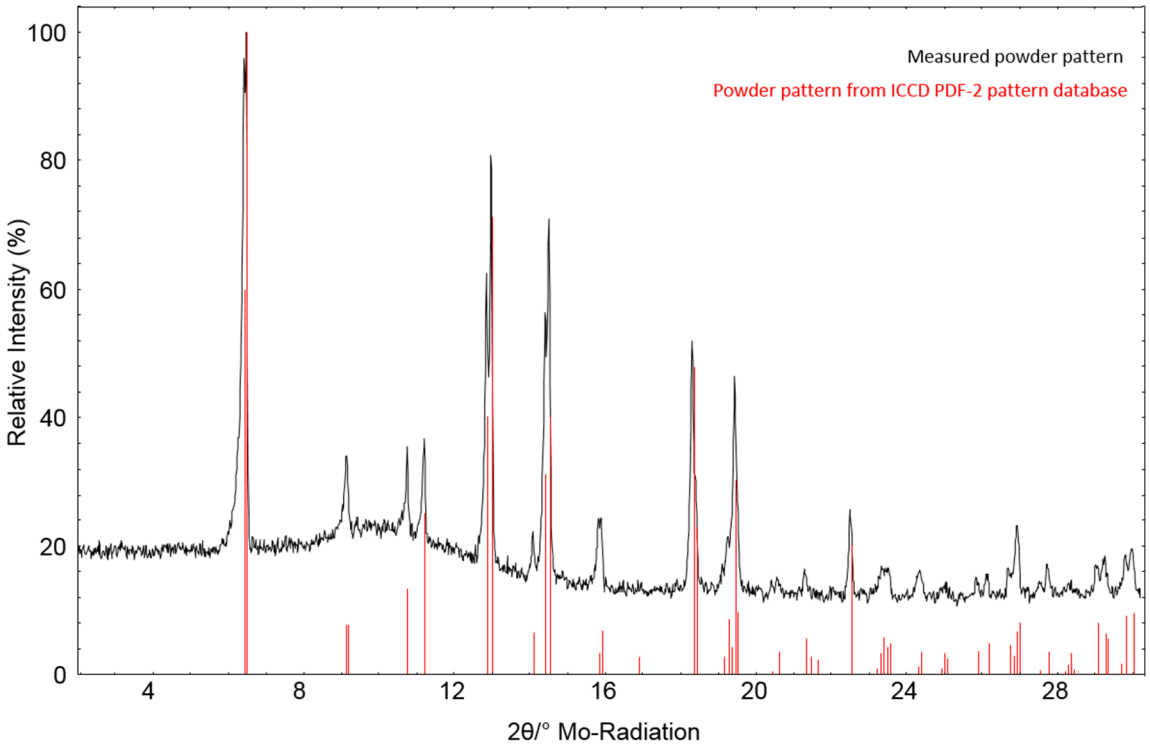

Figure S13. XRD measured (black line) and from the ICCD PDF-2 database powder pattern of MAPI.

References

1. Saidaminov, M. I. *et al.* High-quality bulk hybrid perovskite single crystals within minutes by inverse temperature crystallization. *Nature communications* **6,** 7586; 10.1038/ncomms8586 (2015).